Shipborne polarimetric weather radar:
Impact of ship movement on polarimetric variables

M. Thurai[1], P. T. May[2] and A. Protat[2]

[1]Colorado State Univ., Fort Collins, CO
[2]Center for Australian Weather and Climate Research, Melbourne, Australia

1.   Introduction

Ground based polarimetric radars are providing important new information on cloud microphysics and quantitative precipitation measurement for both research and operational applications (e.g. Bringi and Chandrasekar, 2001). Recent plans now include the operation of polarimetric radar from ships such as the new Australian research vessel, the RV Investigator* that is currently under construction, to allow cloud studies around the globe in key climate regimes ranging from the tropics to the deep Southern Ocean. However, before this can be realized it is necessary to understand the limitations that may be imposed by deployment on a moving platform. While Doppler radar usage on ships is well established, the impact of ship motion on polarimetric radar is less well explored. This paper considers the effect of the ship motion on polarimetric radar variables using scattering simulations at C-band.

---

* Details can be found in: (http://www.marine.csiro.au/ nationalfacility/Investigator/)

2.   Scattering simulations

To assess the impact of ship motion, we can effectively vary the 'apparent' mean canting angles assuming 0 deg elevation. (The effect of elevation angle is considered later). We first consider scattering calculations from a single, oblate rain drop.

(a)   Single scatterers

For scattering calculations from a single scatterer, we refer to Fig. 2.10(a) and equations 2.88(a) and 2.88(c) in Bringi and Chandrasekar (2001). The figure is replicated as Fig. 1 in this paper.
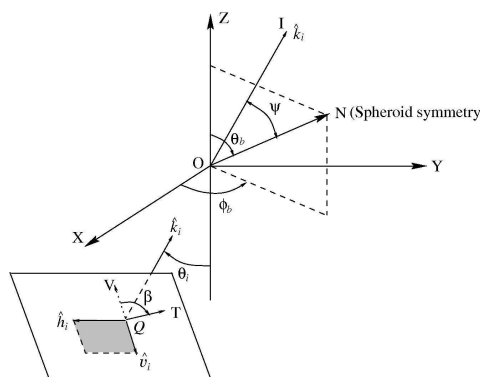

Fig. 1: Reproduction of Fig. 2.10(a) from Bringi and Chandrasekar (2001). The figure is adapted from Holt (1984)

The spheroid symmetry axis is oriented along ON, with angles θ_b and ϕ_b. The angle between the incident direction OI and ON is ψ. For horizontal incidence (i.e. elevation angle zero) and when ON lies in the plane of polarization, the term ψ in equation 2.88(a) and 2.88(c) is equal to $90°$, and they simplify to:

$$(S_{hh})_{BSA} = \frac{k_0^2}{4\pi\varepsilon_0} \left[\alpha_{Zb} \sin^2\beta + \alpha\cos^2\beta \right]$$

(1a)

$$(S_{vv})_{BSA} = \frac{k_0^2}{4\pi\varepsilon_0} \left[\alpha_{Zb} \cos^2\beta + \alpha\sin^2\beta \right]$$

(1b)

respectively, where $(S_{hh})_{BSA}$ and $(S_{vv})_{BSA}$ are the backscatter amplitudes for h and v polarizations, and the term β can be considered as the apparent canting angle and α_{Zb} and α the polarizability of the spheroid along the symmetry axis and in the plane orthogonal to it respectively.

The differential reflectivity z_{dr} in linear units (as ratio) then becomes:

$$z_{dr} = \frac{|S_{hh}|^2}{|S_{vv}|^2} =$$

$$\frac{\alpha_{Zb}^2 \sin^4\beta + \alpha^2 \cos^4\beta + 2\alpha\alpha_{Zb}\sin^2\beta\cos^2\beta}{\alpha_{Zb}^2 \cos^4\beta + \alpha^2 \sin^4\beta + 2\alpha\alpha_{Zb}\sin^2\beta\cos^2\beta}$$

(2)

Note that since

$$z_{dr} = \left(\frac{\alpha}{\alpha_{zb}} \right)^2$$

(3)

equation (2) will eventually become

$$z_{dr} = \frac{\sin^4\beta + z_{dr}\cos^4\beta + \sqrt{z_{dr}}\ 2\sin^2\beta\cos^2\beta}{\cos^4\beta + z_{dr}\sin^4\beta + \sqrt{z_{dr}}\ 2\sin^2\beta\cos^2\beta}$$

(4)

In Fig. 2, we show the variation of Z_{dr} (in dB) with the mean canting angle. The various color curves correspond to Z_{dr} of 5, 4, 3, 2, 1, 0.5 and 0 dB for mean canting angle of 0 deg. Note, at 45 deg, Z_{dr} goes to 0 dB as expected, and beyond that, it becomes negative, once again as expected.
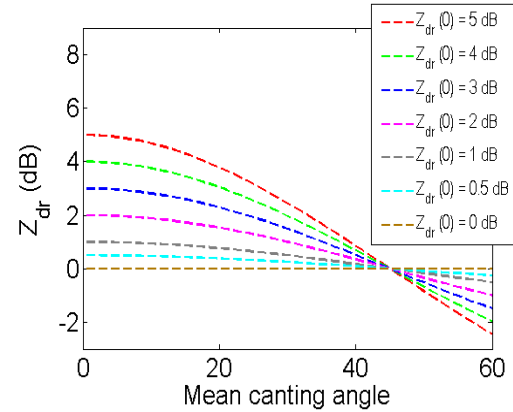

Fig. 2: Variation of Z_{dr} with mean canting angle for a single scatterer. Each color curve represents the various Z_{dr} at 0 deg mean canting angle. (Rayleigh approximation is used).

(b)   Using drop size distribution

For a distribution of scatterers, it is more convenient to use the numerical T-matrix method (derived by Waterman, 1971, and later developed further by Mishchenko et al., 1996) to simulate the canting

angle variation. As input to the scattering calculations, data from a 2D video disdrometer located in SE Queensland have been used. Several hundreds of 1-minute drop size distributions (DSD), with the median volume diameter ranging from 0.5 mm to 3 mm, were used. The mean canting angles were varied as in Fig. 2, and a narrow, Gaussian, canting angle distribution is also assumed with a standard deviation of 5 deg. Additionally, the 'most probable' shapes given in equations (1) and (2) in Thurai et al. (2007) have been used in our calculations.

The resulting variations for C-band are shown in Fig. 3. Each point (black circles) represents the resulting Z_{dr} for each of the 1-minute DSD and an assumed mean canting angle. Superimposed on the plot are the same curves shown in Fig. 2. The single scatter curves cut through the DSD-based simulations – as expected – and at a tilt of 45 deg, Z_{dr} information is lost.
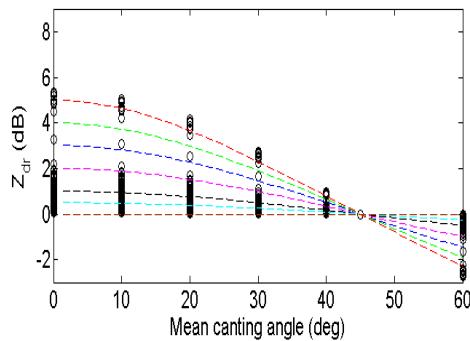

Fig. 3: Calculations using a modified version of the T-matrix program. 1-minute DSDs from disdrometer measurements have been used as Input to the calculations.

To relate the resulting Z_{dr} to the microphysical parameters, we show in Fig. 4(a) the variation of Z_{dr} with the median volume diameter, D_0, for mean canting angles varying from 0 deg to 30 deg. The light yellow points represent the Z_{dr} for zero deg mean canting angle. As expected, D_0 increases with increasing Z_{dr}. The rise in Z_{dr} is particularly high for D_0 values from ~ 2 mm to ~ 2.5 mm. Also note that the decrease in Z_{dr} with canting angle is higher for DSDs with higher D_0 which are often associated with higher rainfall rates. The corresponding changes in LDR are shown in Fig. 4(b). An increase in the cross-polar backscatter is obtained (as expected), with the increase getting higher for larger canting angles, particularly for D_0 values from 2 to 2.5 mm.
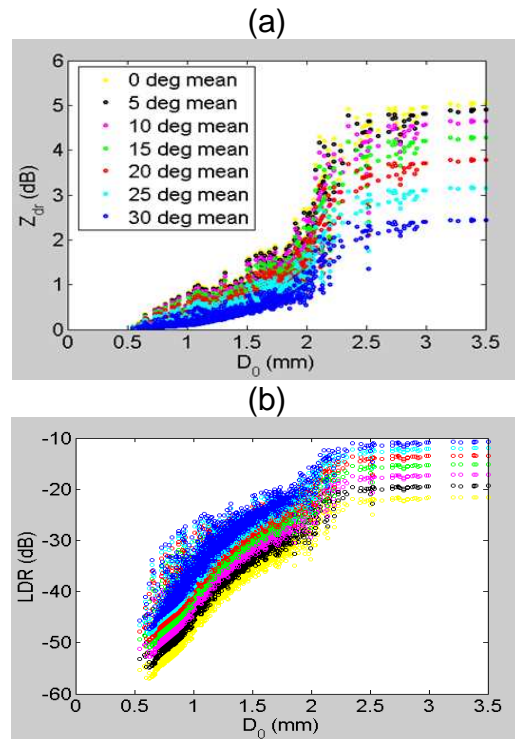
(a)

(b)

Fig. 4: (a) Z_{dr} as a function of median volume diameter and mean canting angle, (b) the corresponding variation in LDR.

3. Other polarimetric variables

The four panels in Fig. 5 summarize the change in the four variables, namely, Z_{dr}, LDR, K_{dp} and ρ_{hv}. The first two parameters are essentially the same as those given in Fig. 4(a) and (b), but represented in terms of the actual parameters for the various mean canting angles versus those for 0 deg mean angle. In all cases except ρ_{hv}, the variation is linear. This is to be expected since the canting angle term in the scattering calculations decouples from the rest of the scattering matrix computations, except for ρ_{hv}.

The simulation results in Fig. 5 show that for an expected ship motion of less than about ± 15 deg, the effects are fairly tolerable. Furthermore, the results from the scattering simulations can potentially be used to determine approximate correction factors to be applied to compensate for the 'apparent' non-zero canting angles.

4. Other considerations

(a) Cross coupling errors

For systems employing simultaneous transmit (& receive), one needs to consider cross-coupling effects between H and V polarizations (Doviak et al. 2000). The errors which arise as a result of non-zero mean canting angles has been quantified by Hubbert et al. (2010). They show that the depolarization-induced Z_{dr} bias at C-band can be significant depending on the principal plane differential propagation phase, Φ_{dp}. For example, for a Φ_{dp} increase of 40 deg at C-band, the Z_{dr} bias can be 2 dB if the mean canting angle is 10 deg, and for circular polarization transmit. For slant 45 deg transmission, the errors are significantly less (at S-band, it was shown to be less than 1 dB).
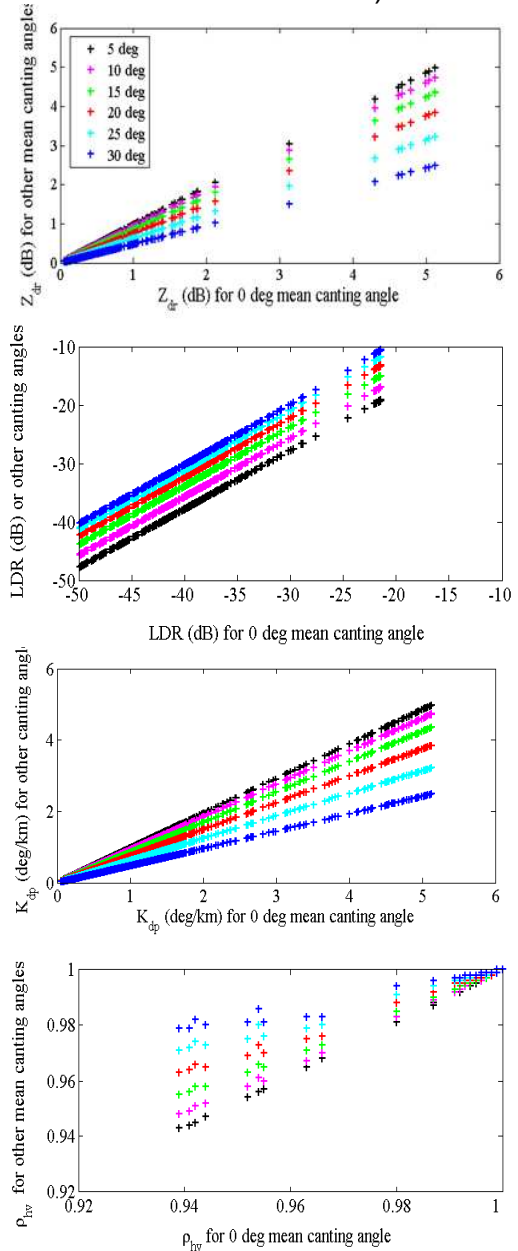

Fig. 5: Variations of the four main polarimteric parameters with the mean canting angle; Zdr (top panel), LDR (second panel), Kdp (third panel) and ρ_{hv} (fourth panel).

(b)   Elevation dependence

Another consideration for ship-borne radar is the variation in the apparent elevation angle. Under Rayleigh approximation, it is possible to correct Z_{dr} for a given radar elevation angle. This correction is less than 0.2 dB for elevation angles less than 10^0, hence, under most circumstances, the DSD parameters or rain fall rates from the radar measurements can be retrieved without having to do any correction for Z_{dr}.

When the elevation angles exceed 10^0, the following equation can be used to convert Z_{dr} at a given elevation angle to Z_{dr} at 0^0 elevation, using the following equation:

$$z_{dr}\left(0^0\right) = \frac{\cos^4(\theta)}{\left[z_{dr}(\theta)^{-0.5} - \sin^2(\theta)\right]^2} \qquad (5)$$

where θ is the elevation angle, and z_{dr} is expressed as ratio. The above equation is only valid for

$$\theta < \theta_{limit} \text{ - } 10^0$$

where θ_{limit} is given by

$$\theta_{\lim it} = \sin^{-1}\left[z_{dr}^{-0.25}(\theta)\right] \qquad (6)$$

Note z_{dr} values are expressed as ratios (as before in eq. (3)), and eq. (5) is valid only for oblate (or rotationally symmetric) raindrops under Rayleigh scattering.

5.   Summary

The deployment of dual polarization radar offers the capability of measuring cloud and precipitation characteristics in areas of key climate and weather importance that are presently poorly sampled. However, before this can be realized it is necessary to understand the limitations that may be imposed by deployment on a moving platform (e.g. ship).   To this end, we have performed scattering calculations for single drops as well as for drop size distribution in rain. Our results show that such deployments are feasible with similar results to land based systems able to be obtained as long as the ship movement is limited to roll of less than about 10 to 15°. The design specification for the RV Investigator is less than 5° of roll with ship stabilization so that good measurements will be obtained with the same limitations regarding simultaneous transmission of H and V polarizations.

Acknowledgments

References

Bringi, V., and V. Chandrasekar, 2001: Polarimetric Doppler Weather Radar. Cambridge University Press, 662 pp.

Doviak, R., V. Bringi, A. Ryzhkov, A. Zahrai, and D. Zrnic´, 2000: Polarimetric upgrades to operational WSR-88D radars. J. Atmos. Oceanic Technol., 17, 257–278.

Holt, A. R., 1984: Some factors affecting the remote sensing of rain by polarization diversity radar in the 3 to 35 GHz range, Radio Science, 19, 1399-1412.

Hubbert, J. C., S. M. Ellis, M. Dixon, G. Meymaris, 2010: Modeling, Error Analysis, and Evaluation of Dual-Polarization Variables Obtained from Simultaneous Horizontal and Vertical Polarization Transmit Radar. Part I: Modeling and Antenna Errors. J. Atmos. Oc. Technol., 27, 1583–1598.

Mishchenko, M. I., L. D. Travis, and D. W. Mackowski, 1996: T-matrix computations of light scattering by nonspherical particles: A review. J. Quant. Spectrosc. Radiat. Transfer, 55, 535–575.

Thurai, M., G-J. Huang, V. N. Bringi, W. L. Randeu, M. Schönhuber, 2007: Drop Shapes, Model Comparisons, and Calculations of Polarimetric Radar Parameters in Rain. J. Atmos. Oceanic Technol., 24, 1019–1032.

Waterman, P. C., 1971: Symmetry, unitarity, and geometry in electromagnetic scattering. Phys. Rev. D, 3, 825.